Genetic Control of Surface Curvature

Utpal Nath, Brian C. W. Crawford, Rosemary Carpenter, Enrico Coen*

Although curvature of biological surfaces has been considered from mathematical and biophysical perspectives, its molecular and developmental basis is unclear. We have studied the *cin* mutant of *Antirrhinum*, which has crinkly rather than flat leaves. Leaves of *cin* display excess growth in marginal regions, resulting in a gradual introduction of negative curvature during development. This reflects a change in the shape and the progression of a cell-cycle arrest front moving from the leaf tip toward the base. *CIN* encodes a TCP protein and is expressed downstream of the arrest front. We propose that *CIN* promotes zero curvature (flatness) by making cells more sensitive to an arrest signal, particularly in marginal regions.

The extent to which a surface is curved can be expressed in terms of Gaussian curvature, the product of curvature in orthogonal directions (*1*–*3*). A flat surface growing isotropically, such as a uniformly expanding disk, maintains zero Gaussian curvature (Fig. 1A). However, if marginal regions grow more slowly than the center, the disk will adopt a cup shape that has positive Gaussian curvature. Conversely, if the marginal areas grow more rapidly, the disk will buckle to form a shape with a wavy edge, such as a saddle, with negative Gaussian curvature. Studies on surface curvature from mathematical (*4*, *5*) and biophysical viewpoints (*6*, *7*) have raised the question of what role, if any, genes play in the control of curvature.

Some organs, such as leaves of many plants or insect wings, are flat or can be flattened without making cuts or folds, indicating that they have approximately zero Gaussian curvature. Although such flatness is often taken for granted, the probability of this happening by chance is low because there are many more ways for a structure to adopt negative or positive curvature than zero curvature (Fig. 1A). This suggests that the extent of curvature should be under genetic control. Consistent with this theory, several mutants have been described in which wings or leaves are crinkly (*8*–*10*). However, the mechanisms by which these genes influence curvature have not been addressed. We have studied this problem by analyzing *CINCINNATA* (*CIN*), a gene that affects leaf curvature in *Antirrhinum*.

CIN was identified through inactivation of a gene belonging to the TCP family of DNA binding proteins (Fig. 1B and fig. S1) (*11*–*13*). Members of the TCP family are involved in various developmental processes in plants (*14*–*16*). A reverse genetic screen (*17*) of the TCP gene yielded three insertion and two deletion alleles (Fig. 1C). Both deletion alleles were recessive and gave a homozygous phenotype similar to that of two previously described mutants (*9*): *cincinnata* (*cin*) and

Department of Cell and Developmental Biology, John Innes Centre, Norwich Research Park, Norwich, NR4 7UH, UK.

*To whom correspondence should be addressed. E-mail: enrico.coen@bbsrc.ac.uk

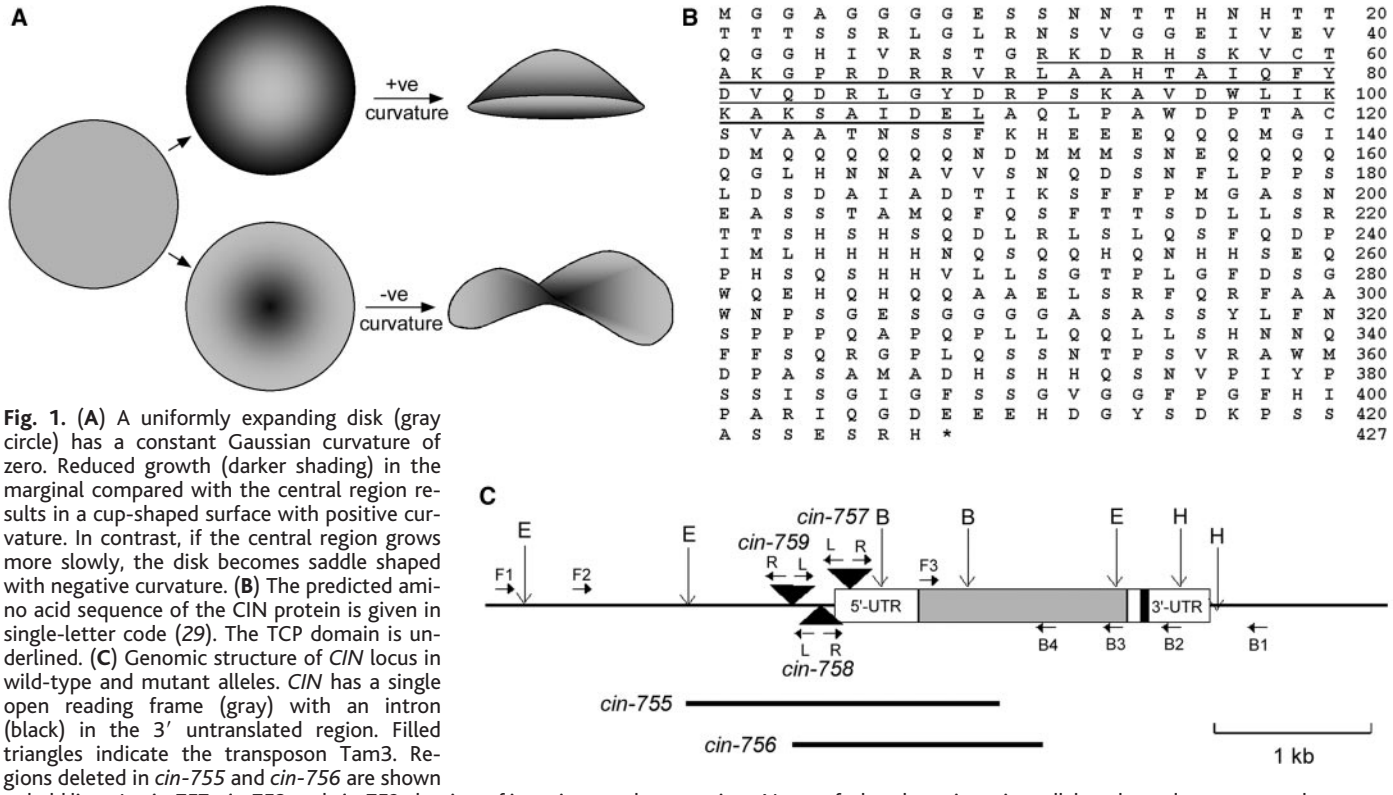

Fig. 1. (**A**) A uniformly expanding disk (gray circle) has a constant Gaussian curvature of zero. Reduced growth (darker shading) in the marginal compared with the central region results in a cup-shaped surface with positive curvature. In contrast, if the central region grows more slowly, the disk becomes saddle shaped with negative curvature. (**B**) The predicted amino acid sequence of the CIN protein is given in single-letter code (*29*). The TCP domain is underlined. (**C**) Genomic structure of *CIN* locus in wild-type and mutant alleles. *CIN* has a single open reading frame (gray) with an intron (black) in the 3′ untranslated region. Filled triangles indicate the transposon Tam3. Regions deleted in *cin-755* and *cin-756* are shown as bold lines. In *cin-757*, *cin-758*, and *cin-759*, the sites of insertion are about 400, 600, and 900 base pairs (bp) upstream of the initial ATG, respectively, as determined by polymerase chain reaction (PCR) analysis. In *cin-755* and *cin-756*, the deletions extend from −1532 to +390 bp and −852 to +716 bp, respectively, relative to the initial ATG, as determined by DNA sequencing. None of the three insertion alleles showed a mutant phenotype, whereas both deletion alleles showed phenotypes similar to the two classical alleles, cin^{cin} and cin^{suba}. Arrows indicate the sites of forward (F1 to F3) and backward (B1 to B4) primers used for PCR screening. L and R indicate left-end and right-end primers of Tam3. E, Eco RI; B, Bam HI; H, Hind III.

subcrispa (*suba*). These mutants have flowers with reduced petal lobes and leaves with a crinkly lamina. Crosses showed that *cin* and *suba* were allelic to each other and to the deletions. Moreover, both *cin* and *suba* had alterations in the coding region of the TCP gene (*18*). This implied that the same locus, named *CIN* after its first representative, had been affected in all cases.

Three aspects of leaf geometry were affected in *cin* mutants: shape, size, and curvature (Figs. 2 and 3). The lamina of a mature wild-type leaf has an elliptical shape, whereas that of a mature *cin* leaf is rounder (Fig. 2) (see length-to-width ratio in Table 1). This difference in shape first became apparent when the leaves were about 10 mm long (Figs. 2C and 3A). The rate of growth in width was similar for the *cin* and the wild type. However, the *cin* leaves grew for a longer period of time (Fig. 3B), resulting in a greater final width and total area (Table 1).

Although a mature wild-type *Antirrhinum* leaf can show mild downward curvature, it can be flattened without introducing any cuts or folds and therefore has overall zero Gaussian curvature. By contrast, mature *cin* leaves could not be flattened without introducing folds, indicating overall negative curvature. The extent of curvature was estimated from the excess area within the folds (Fig. 2C, dark patches). Negative curvature appeared in the *cin* mutant after the leaves were about 20 mm long and increased steadily thereafter until maturity (Fig. 3C). In addition, the *cin* mutants showed local bulging of lamina on the abaxial (ventral) side, in between leaf veins (Fig. 2B, arrow), indicating an excess of growth in intervein regions.

The perimeter of the *cin* leaves was about 50% greater than the perimeter of the wild type (Table 1). To test whether this might account for negative curvature, we measured the leaf perimeter (P) at various stages relative to total leaf area (A). For a perfect circular leaf, $P/\sqrt{A}$ is $2\pi r/\sqrt{\pi r^2} \approx 3.55$. For wild-type leaves, $P/\sqrt{A}$ was slightly greater than this, measuring 3.8 (Table 1), as expected from their elliptical shape (Fig. 3D). For the *cin* mutants, $P/\sqrt{A}$ was initially similar to the wild-type value but started increasing after the leaf was ~30 mm long, to a maximum of 5.0 at maturity, even though the length-to-width ratio continued to remain at about 1.0. This showed that the perimeter of *cin* grew faster than a circular shape could accommodate, consistent with negative curvature.

To determine whether excess growth of the *cin* mutant leaves arose through changes in cell division or expansion, we compared cell sizes near the margins of wild-type and mutant leaves. Cells usually remain small during proliferation but increase in size following the arrest of division, when further growth is accommodated by cell expansion. In young wild-type leaves, cells throughout the leaf were relatively small. By the time the leaf was about 3 mm long, cells near the tip started to increase in size, reflecting an early arrest of division (Fig. 3E). Shortly after this, cells in the middle of the leaf also started to increase in size, indicating that these cells underwent arrest at a slightly later stage than those at the tip. Cells in proximal regions remained small for the longest period. This behavior is consistent with a front of cell-cycle arrest moving gradually from the leaf tip to base, as described in other species (*19–25*). Cells in the proximal and distal regions of the *cin* leaves showed a pattern of cell size changes similar to that of the wild type. However, cells in the middle region showed a delay in cell-size increase, indicating that progression of the arrest front through this region was delayed (Fig. 3F).

We further examined the progression of the arrest front by analyzing the expression pattern of *HISTONE4* (*H4*). *H4* expression varies during the cell cycle such that only a proportion of cells give a strong signal in proliferating tissue (*26*). In the wild type, a decline in the proportion of cells expressing *H4* was detected at the tip of young leaves, and this decline moved progressively toward the base during later stages, confirming the movement of a graded arrest front from the tip toward the base (Fig. 4A). In the *cin* mutants, the decline of *H4* proceeded more slowly through the middle region of the leaf compared with that in the wild type, and had a strongly concave rather than weakly convex shape (Fig. 4B). Expression of *CYCLIN D3b*, a key regulator of the cell cycle in plants (*27*), showed a parallel pattern (Fig. 4C), although the decline in expression was detected more proximally, reflecting the lower abundance of *CYCLIN D3b* relative to *H4* (*28*).

These effects on the progression and shape

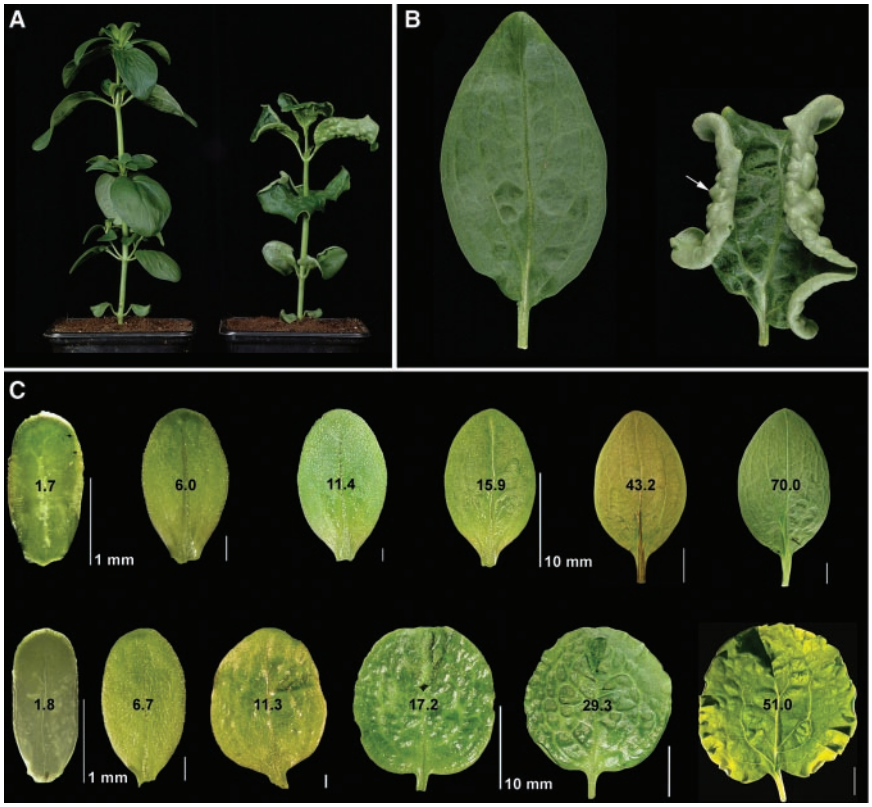

Fig. 2. Phenotype of wild-type and *cin-756* plants. (**A**) One-month-old wild-type (left) and *cin-756* (right) plants. (**B**) Mature leaves at the fourth node of wild-type (left) and *cin-756* (right) plants. Arrow indicates bulge between veins. (**C**) Stages of wild-type (upper row) and *cin-756* (lower row) leaves scaled to the same length. Numbers in black show leaf lamina lengths in millimeters. Scale bars are 1 mm for the first three leaves and 10 mm for the last three leaves.

Table 1. Measurements of mature wild-type and *cin* leaf laminae. Each data point is the mean (±SD) of measurements from at least eight leaves at the fourth node (cotyledon corresponds to first node).

	Length (mm)	Width (mm)	Perimeter (mm)	Area (mm^2)	Length/ width	Perimeter/ $\sqrt{area}$
Wild type	64 ± 3	42 ± 1.3	168 ± 4.3	1990 ± 130	1.5	3.8
cin	51 ± 5	53 ± 3	260 ± 33	2670 ± 352	1.0	5.0

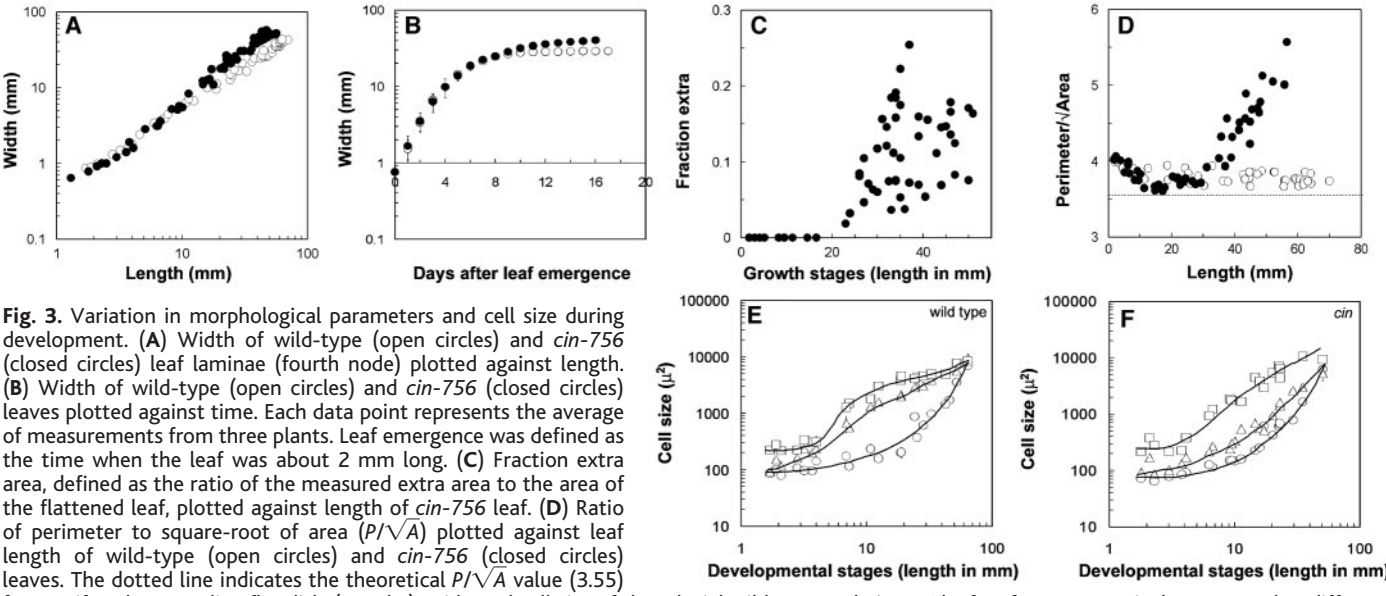

Fig. 3. Variation in morphological parameters and cell size during development. (**A**) Width of wild-type (open circles) and *cin-756* (closed circles) leaf laminae (fourth node) plotted against length. (**B**) Width of wild-type (open circles) and *cin-756* (closed circles) leaves plotted against time. Each data point represents the average of measurements from three plants. Leaf emergence was defined as the time when the leaf was about 2 mm long. (**C**) Fraction extra area, defined as the ratio of the measured extra area to the area of the flattened leaf, plotted against length of *cin-756* leaf. (**D**) Ratio of perimeter to square-root of area ($P/\sqrt{A}$) plotted against leaf length of wild-type (open circles) and *cin-756* (closed circles) leaves. The dotted line indicates the theoretical $P/\sqrt{A}$ value (3.55) for a uniformly expanding flat disk. (**E** and **F**) Epidermal cell size of the adaxial wild-type and *cin-756* leaf surfaces, respectively, measured at different developmental stages and plotted against leaf length. Cells from marginal regions were measured near the tip (squares), middle (triangles) and base (circles) of the leaf. Each data point represents the average of one to three measurements, and the coefficient of variation ranged from 2 to 15%.

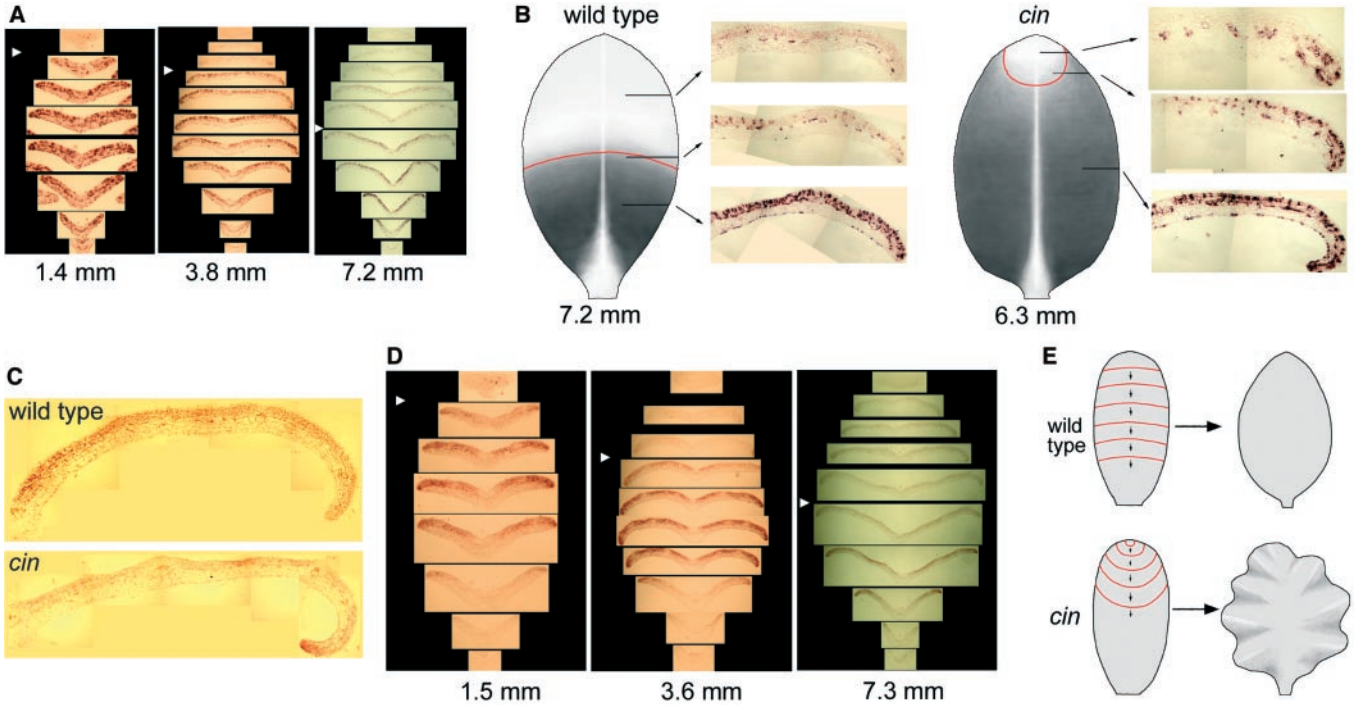

Fig. 4. Expression pattern of *H4*, *CYCLIN D3b*, and *CIN* in developing wild-type and *cin-756* leaves. (**A**) Transverse sections showing decline in the proportion of cells displaying *H4* expression from the tip to the base during leaf growth. Sections are arranged from the base (bottom) to the tip (top) of the leaf proportional to leaf length. Arrowheads indicate the extent to which the decline in proportion of cells expressing *H4* appears to have progressed from the tip. Numbers indicate leaf lamina length. (**B**) Schematic representation of *H4* expression in a young leaf together with sections showing *H4* expression. In *cin-756*, the region expressing *H4* (dark shading) is larger and has a concave rather than convex boundary (red lines) compared to wild type. Horizontal black lines indicate the positions of the sections shown. The leaves have been reconstructed from the measurements of the serial sections. *H4* is expressed in a high proportion of cells at the base of the lamina. This proportion gradually declines toward the tip. (**C**) Transverse sections through the middle of young leaves (6 to 7 mm lamina length) showing *CYCLIN D3b* expression (only right half of the section has been shown). Expression is stronger in the medial region in wild type and in the margin in *cin-756*. (**D**) *CIN* is expressed in the lamina, proximal to the arrest front (arrowhead), based on adjacent sections probed with *H4*. As the leaf grows, the decline in expression progressively moves from the tip to the base. Transverse sections have been arranged as in (A). Numbers indicate leaf lamina length. (**E**) Schematic illustration of progression of arrest front (red lines) in developing leaves (left). In wild type, the arrest front is weakly convex, resulting in an elliptical final leaf shape (right) with zero Gaussian curvature. In *cin* mutants, the arrest front is concave and initially progresses more slowly down the leaf. This progression results in greater growth in marginal regions, leading to a broader leaf with negative curvature. The shape on the left is based on a 1.5-mm leaf.

of the arrest front can largely account for the effects of *CIN* on leaf morphology. Because the arrest front moves more slowly and is changed from weakly convex to strongly concave, the marginal regions of the *cin* leaf grow for a longer period relative to medial regions, both in width and length. The extra growth in width leads to a wider leaf, whereas the extra growth in length, parallel to the leaf periphery, introduces negative curvature.

To determine where *CIN* is expressed relative to the arrest front, we carried out RNA in situ hybridizations. In young leaves, expression was restricted to the adaxial side, was stronger in marginal than medial regions, and was absent from veins. *CIN* expression eventually declined from tip to base (Fig. 4D), in parallel with the decline of *H4* and *CYCLIN D3b* expression. Thus, *CIN* is expressed in the actively dividing region of the leaf lamina, proximal to, and perhaps overlapping, the arrest front. This suggests that *CIN* may act by modifying the response of cells to arrest signals, perhaps through regulation of cell-cycle gene expression. This effect seems to be local, because the regions that normally express *CIN* (interveins) show excess growth in the *cin* mutants compared with those that do not (veins).

In *cin* mutants, arrest spreads out from the leaf tip with an almost circular front (Fig. 4B). This would result in an excess of growth in the margins because they would continue to proliferate when the more medial regions have arrested. *CIN* could counteract this by making cells more sensitive to the arrest signal, particularly in marginal regions where it is more strongly expressed. This would effectively straighten and accelerate the arrest front, ensuring that zero curvature is maintained while leaf growth is progressively arrested. This suggests that an important element in the control of leaf flatness lies in precise genetic regulation of the pattern of cell-cycle arrest.

References and Notes

1. P. H. Todd, *J. Theor. Biol.* **113**, 63 (1985).
2. P. Krsek, G. Lukacs, R. R. Martin, in *The Mathematics of Surfaces*, R. Cripps, Ed. (Clarendon, Oxford, 1998), pp. 1–16.
3. J. Dumais, D. Kwiatkowska, *Plant J.* **31**, 229 (2002).
4. M. Marder, *Cond. Mat.*, in press; preprint available at http://xxx.lanl.gov/abs/cond-mat/0208232.
5. P. Ball, *Nature Science Update*, www.nature.com/nsu/020819/020819-3.html (21 August 2002).
6. P. B. Green, *Ann. Bot.* **78**, 269 (1996).
7. _____, *Am. J. Bot.* **86**, 1059 (1999).
8. C. H. Waddington, *J. Genet.* **41**, 75 (1940).
9. H. Stubbe, *Genetik und Zytologie von Antirrhinum* L. sect *Antirrhinum* (Veb Gustav Fischer Verlag, Jena, Germany, 1966).
10. A. Garcia-Bellido, *Ciba Found. Symp.* **0**, 161 (1975).
11. S. Kosugi, Y. Ohashi, *Plant Cell* **9**, 1607 (1997).
12. P. Cubas, N. Lauter, J. Doebley, E. Coen, *Plant J.* **18**, 215 (1999).
13. S. Kosugi, Y. Ohashi, *Plant J.* **30**, 337 (2002).
14. D. Luo, R. Carpenter, C. Vincent, L. Copsey, E. Coen, *Nature* **383**, 794 (1996).
15. J. Doebley, A. Stec, L. Hubbard, *Nature* **386**, 485 (1997).
16. D. Luo *et al.*, *Cell* **99**, 367 (1999).
17. Materials and methods are available as supporting material on *Science* Online.
18. B. C. W. Crawford, U. Nath, R. Carpenter, E. Coen, unpublished results.
19. G. S. Avery Jr., *Am. J. Bot.* **20**, 565 (1933).
20. R. S. Poethig, I. M. Sussex, *Planta* **165**, 170 (1985).
21. _____, *Planta* **165**, 158 (1985).
22. S. D. Wolf, W. K. Silk, R. E. Plant, *Am. J. Bot.* **73**, 832 (1986).
23. A. W. Sylvester, W. Z. Cande, M. Freeling, *Development* **110**, 985 (1990).
24. K. A. Pyke, J. L. Marrison, R. M. Leech, *J. Exp. Bot.* **42**, 1407 (1991).
25. P. M. Donnelly, D. Bonetta, H. Tsukaya, R. Dengler, N. G. Dengler, *Dev. Biol.* **215**, 407 (1999).
26. P. R. Fobert, E. S. Coen, G. J. Murphy, J. H. Doonan, *EMBO J.* **13**, 616 (1994).
27. V. Gaudin *et al.*, *Plant Physiol.* **122**, 1137 (2000).
28. J. H. Doonan, personal communication.
29. Single-letter abbreviations for the amino acid residues are as follows: A, Ala; C, Cys; D, Asp; E, Glu; F, Phe; G, Gly; H, His; I, Ile; K, Lys; L, Leu; M, Met; N, Asn; P, Pro; Q, Gln; R, Arg; S, Ser; T, Thr; V, Val; W, Trp; and Y, Tyr.

30. We thank D. Bradley for critical comments on the manuscript. A *CIN* cDNA was kindly provided by Z. Schwarz-Sommer, Max Planck Institute, Köln, Germany. The *Antirrhinum* genomic library was provided by H. Sommer, Max Planck Institute, Köln, Germany. The Matlab program was written by A.-G. Rolland, University of East Anglia, Norwich, UK. This work was supported by the Biotechnology and Biological Sciences Research Council and Gatsby Charitable Foundation. U.N. was supported by The Rockefeller Foundation and the Human Frontier Science Program Organization. The *CIN* nucleotide sequence has been deposited in GenBank (accession number AY205603).

Supporting Online Material

www.sciencemag.org/cgi/content/full/299/5611/1404/DC1
Materials and Methods
Fig. S1
References and Notes

11 October 2002; accepted 2 January 2003

Steroid Control of Longevity in *Drosophila melanogaster*

Anne F. Simon, Cindy Shih, Antha Mack, Seymour Benzer*

Ecdysone, the major steroid hormone of *Drosophila melanogaster*, is known for its role in development and reproduction. Flies that are heterozygous for mutations of the ecdysone receptor exhibit increases in life-span and resistance to various stresses, with no apparent deficit in fertility or activity. A mutant involved in the biosynthesis of ecdysone displays similar effects, which are suppressed by feeding ecdysone to the flies. These observations demonstrate the importance of the ecdysone hormonal pathway, a new player in regulating longevity.

In humans, changes in steroid hormones occur during aging (*1*), but whether those changes are a cause or an effect of aging remains unclear. To investigate the role of steroids in the aging process, we used genetics to manipulate a steroid hormone in adult *Drosophila* flies.

Steroid hormones in insects are ecdysteroids, and the major form in *Drosophila* is ecdysone. Its active metabolite, 20-OH-ecdysone, is important in developmental transitions and metamorphosis in *Drosophila melanogaster* (*2*). Ecdysone is also involved in oogenesis in the adult fly, but other functions are not known (*2*, *3*). 20-OH-ecdysone circulates and binds to a heterodimeric nuclear receptor consisting of an ecdysone receptor (EcR) and Ultraspiracle (USP), a homolog of the retinoid X receptor (RXR) (*2*). In the absence of ecdysone, the EcR-USP heterodimer is thought to form a complex with one or more corepressor proteins (N-CoR and SMRT), which bind to chromosomal histone deacetylases (Sin3A/Rpd3) (*2*, *4*). When the ligand is bound to the receptor, the complex binds instead to coactivators that recruit histone acetyltransferases, thus activating the transcription of various genes, including transcription factors (*5*), chaperones (*6*), apoptosis genes (*7*), and catalase (*8*). We investigated the role of ecdysone during adulthood by studying flies with mutations in *EcR* (*9*) and in a gene involved in ecdysone biosynthesis, *DTS-3* (*10*).

The *EcR* gene encodes three isoforms. We first studied a mutant, EcR^{V559fs}, which has a 37–base pair deletion in the predicted ligand-binding domain in a region common to the three isoforms (*9*). It is homozygous lethal during development but adult viable as a heterozygote. $EcR^{V559fs}/+$ flies lived longer than the controls (Fig. 1); male and female average life-spans increased by 40 to 50%. This was true for heterozygous offspring of crosses between two independent *cinnabar brown* (*cn bw*) backgrounds: the parental line from the Bender laboratory and a *cn bw* from our own laboratory stock. The same increase in longevity was observed, regardless of whether the male or female parents were mutant for EcR^{V559fs}. Progeny of the two *cn bw* lines crossed with each other showed no differences in longevity from the two parental lines.

Developmental time and weight of the adult flies in $EcR^{V559fs}/+$ were equivalent to those of control flies (Fig. 2, A and B). However, $EcR^{V559fs}/+$ flies showed increased resistance to three stresses: oxidative challenge, heat, and dry starvation (Fig. 2C). The $EcR^{V559fs}/+$ were also more active than controls, as measured by their performance in

Division of Biology 156-29, California Institute of Technology, 1201 California Boulevard, Pasadena, CA 91125, USA.

*To whom correspondence should be addressed. E-mail: benzer@caltech.edu